Resilience and vulnerabilities of tumor cells under purine shortage stress

Jianpeng Yu[1]*, Chen Jin[1]*, Cheng Su[1], David Moon[1], Michael Sun[1], Hong Zhang[1], Xue Jiang[1], Fan Zhang[1], Nomi Tserentsoodol[1], Michelle L. Bowie[2,3], Christopher J Pirozzi[1,2], Daniel J. George[4], Robert Wild[5], Xia Gao[6,7], David M Ashley[2,3], Yiping He [1,2,#], Jiaoti Huang[1,#]

[1]Department of Pathology, Duke University School of Medicine, Durham, North Carolina, USA
[2]The Preston Tisch Brain Tumor Center, Duke University, Durham, North Carolina, USA
[3]Department of Neurosurgery, Duke University School of Medicine, Durham, North Carolina, USA
[4]Department of Medicine, Duke University School of Medicine, Durham, North Carolina, USA
[5]Dracen Pharmaceuticals, Inc., San Diego, California, USA
[6]Department of Molecular and Cellular Biology, Baylor College of Medicine, Houston, Texas, USA
[7]USDA/ARS Children's Nutrition Research Center, Department of Pediatrics, Baylor College of Medicine, Houston, Texas, USA

*These authors contributed equally
[#]Corresponding:

Jiaoti Huang, MD, PhD
Jiaoti.huang@duke.edu

Yiping He, PhD
yiping.he@duke.edu

Keywords: prostate cancer, purine biosynthesis, MTAP, glioma, DRP-104

Abstract

Purine metabolism is a promising therapeutic target in cancer; however how cancer cells respond to purine shortage,particularly their adaptation and vulnerabilities, remains unclear. Using the recently developed purine shortage-inducing prodrug DRP-104 and genetic approaches, we investigated these responses in prostate, lung and glioma cancer models. We demonstrate that when de novo purine biosynthesis is compromised, cancer cells employ microtubules to assemble purinosomes, multi-protein complexes of de novo purine biosynthesis enzymes that enhance purine biosynthesis efficiency. While this process enables tumor cells to adapt to purine shortage stress, it also renders them more susceptible to the microtubule-stabilizing chemotherapeutic drug Docetaxel. Furthermore, we show that although cancer cells primarily rely on de novo purine biosynthesis, they also exploit Methylthioadenosine Phosphorylase (MTAP)-mediated purine salvage as a crucial alternative source of purine supply, especially under purine shortage stress. In support of this finding, combining DRP-104 with an MTAP inhibitor significantly enhances tumor suppression in prostate cancer (PCa) models in vivo. Finally, despite the resilience of the purine supply machinery, purine shortage-stressed tumor cells exhibit increased DNA damage and activation of the cGAS-STING pathway, which may contribute to impaired immunoevasion and provide a molecular basis of the previously observed DRP-104-induced anti-tumor immunity. Together, these findings reveal purinosome assembly and purine salvage as key mechanisms of cancer cell adaptation and resilience to purine shortage while identifying microtubules, MTAP, and immunoevasion deficits as therapeutic vulnerabilities.

Introduction

Glutamine is a major source of carbon for cells and also provides nitrogen for the synthesis of nucleotides and other molecules to promote cancer progression [1 - 5]. Our previous work has established glutamine as a key driver of prostate cancer (PCa) and highlighted both the therapeutic potential and, more importantly, the challenges of effectively targeting its metabolism [6,7]. DON (6-diazo-5-oxo-norleucine), a glutamine antagonist that broadly and irreversibly inhibits multiple enzymes involved in glutamine metabolism, has demonstrated broad anti-tumor activity in patients**.** However, its clinical utility is limited by gastrointestinal toxicity [8]. Recently, prodrugs of DON have been developed that are inactive in normal cells but converted to functional DON in tumor cells due to the increased expression of certain enzymes in tumors [8-10]. Specifically, one such prodrug, DRP-104 (Sirpiglenastat), has shown therapeutic efficacy in lymphoma, colorectal cancer, lung cancer, and pancreatic cancer models, and has been fast-tracked by the FDA for treating non-small cell lung cancer [10-13].

Advanced, hormone-sensitive PCa can be treated with hormonal therapy that inhibits androgen receptor (AR) functions. However the tumor eventually recurs as castration-resistant PCa (CRPC). Most CRPCs retain an adenocarcinoma histology and respond to newer AR antagonists such as enzalutamide, although resistance inevitably develops [14-18]. Some CRPCs are histologically classified as small cell carcinoma or neuroendocrine (NE) PCa (namely NEPC), which are rapidly lethal due to lack of effective treatments[19]. The challenge in treating PCa is further compounded by its extreme intra-tumor heterogeneity. For instance, adenocarcinomas frequently also contain NE-like tumor cells [20], and even cancers in the hormone-sensitive stage harbor pre-existing CRPC-like cells that are destined for therapy resistance and tumor progression[21]. These features contribute to hormonal therapy failure and underscore the urgent need to develop novel, AR-independent therapies.

We have shown that advanced PCa is addicted to glutamine and inhibition of glutamine catabolism has the potential to be an effective, AR-independent therapeutic strategy [6,7]**.** We have shown that DRP-104, a pan glutamine antagonist, inhibits PCa growth with minimal toxicity to normal tissues [22]. While the DRP-104-derived effector metabolite, DON, is expected to disrupt at least seven glutamine-utilizing pathways by inhibiting as many as 10 enzymes [23-32], it remains unclear which of these pathways are most critical to tumor survival. Addressing this question can guide the development of novel treatments and help identify patients who may benefit most from specific therapies. In this context, recent studies, including ours, have demonstrated that DRP-104 effectively disrupts purine supply in tumor cells[12,22]. These findings, along with prior observations that among DON's pharmacological targets, the de novo purine biosynthesis enzyme FGAMS is the most sensitive to inhibition (with the lowest Ki) [23-32], nominate DRP-104 as a potential blocker of purine supply (i.e., an inducer of purine shortage stress). Since purines are essential building blocks and energy sources for cancer cells, purine biosynthesis, primarily de novo purine biosynthesis, has been explored for cancer treatment [33]. Purine shortage can be induced by certain anti-cancer drugs such as Methotrexate, an inhibitor of Dihydrofolate Reductase (DHFR), although toxicity remains a major limitation [34]. The establishment of DRP-104, a low-toxicity prodrug, as an inducer of purine shortage thus provides a new avenue for targeting purine metabolism in cancer cells.

While disrupting purine supply effectively suppresses tumor cell proliferation in experimental models, complete purine depletion in tumor cells is not practical in the clinical setting. Instead, it is more likely that therapies will induce purine shortage rather than total depletion. Thus, elucidating how cancer cells respond to purine shortage, including their adaptive mechanisms and vulnerabilities under such stress, is critical for improving therapeutic designs.In this study we demonstrate that upon purine shortage, cancer cells employ microtubules to assemble complexes resembling purinosomes, in which de novo purine biosynthesis enzymes, along with heat shock proteins (HSP70 and HSP90), form multi-subunit macromolecular complexes as an adaptive mechanism to enhance purine biosynthesis [35-40]. Additionally, we show that cancer cells utilize 5-Methylthioadenosine phosphorylase (MTAP)-dependent purine salvage pathway as an alternative source of purine supply both in purine-rich conditions, and more prominently, during purine shortage stress when de novo purine biosynthesis is compromised. Consequently, the therapeutic efficacy of DRP-104 can be enhanced by inhibiting MTAP, as the combination of DRP-104 with MTAP inhibition results in superior anti-tumor effects in vivo. Finally, despite the versatility and resilience of cancer cells' purine supply machinery, we find that purine shortage-stressed tumor cells display higher levels of DNA damage and activation of the cytosolic double-stranded DNA-sensing cGAS-STING- pathway, indicating compromised immune-evasive ability and providing a mechanistic explanation for the previously observed DRP-104-augmented anti-tumor immune response in several tumor models [10-13]. Collectively, these results highlight cancer cells' resilience to purine shortage stress while identifying microtubules, MTAP-mediated purine salvage, and impaired immunoevasion as therapeutically targetable vulnerabilities. As microtubules are targets of several commonly used chemotherapeutic drugs and homozygous *MTAP* loss occurs commonly in cancers, our observations may represent a general metabolic mechanism that can be exploited for the treatment of multiple cancer types.

Materials and Methods

Sex as a biological variable. Our study exclusively examined male mice since the prostate cancer model is only relevant in males.

Cell lines and cell cultures Prostate cancer cell lines (C4-2, PC3, NCI-H660, and TrampC2) and lung cancer cell line NCI-H358 were purchased from the American Type Culture Collection (ATCC) via Duke Cell Culture Facility (CCF). The cell lines' STR profiles were confirmed by Duke CCF, and the cell lines were tested periodically to ensure that they were mycoplasma-free. All human prostate cancer cell lines were cultured as previously described [22]. Briefly, C4-2 and PC3 cells were maintained in RPMI 1640 medium with L-glutamine (Gibco, 11875093, ThermoFisher, Waltham, MA, USA), supplemented with 10% fetal bovine serum and 1% penicillin-streptomycin. NCI-H660 cells were maintained in stem cell media (Advanced DMEM/F-12 supplemented with X1 B-27 supplement, 10 ng/mL FGF-2, 10 ng/mL EGF, X1 Glutamax, X1 streptomycin and penicillin). TrampC2 cells were maintained in DMEM with L-glutamine (Gibco, 11965092, ThermoFisher), supplemented with 10% fetal bovine serum, 0.005 mg/ml human insulin, and 10 nM dehydroisoandrosterone and 1% penicillin-streptomycin. NCI-H358 cells were maintained in RPMI 1640 medium (Gibco, 11875093, ThermoFisher), supplemented with 10% fetal bovine serum and 1% penicillin-streptomycin. Glioma CT-2A and GL261 (Redflu-tagged) cell lines (generous gifts from Drs. Darrell Bigner and Vidyalakshmi Chandramohan, Duke University) were cultured as in the previous study [41]. The *Mtap* knockout CT-2A line was previously described [42]. The *Mtap*-null derivative GL261 lines were generated following previously described procedure for *Mtap* [42]. DRP-104 adaptive cells were generated by treating parental cell lines with DRP-104 (generally in the range of 2-4 µM) to obtain populations that ultimately developed adaptation as defined by their continuous propagation in the presence of this prodrug. In general, it takes 3-4 weeks to obtain such "adaptive" cells, which were subsequently maintained in DRP-104-containing media.

Chemicals and antibodies DRP-104 and DON were previously described[22]. MTDIA was obtained from

MedKoo Biosciences, Inc (cat# 407244) or from MedChemExpress (cat# HY-101496). Antibodies used for immunohistochemistry included the following: CD3 (1:100 dilution; PB9093, BOSTER, USA), CD8⍰ (1:100 dilution; A02236-1, BOSTER, USA), PD-1 (1:100 dilution; A00178, BOSTER, USA), PD-L1 (1:500 dilution; 17952-1-AP, Proteintech, USA), p-IRF3 (Ser396) (1:50 dilution; MA5-14947, Themo Fisher), and γ-H2AX (1:50 dilution; 9718, Cell Signaling Technology). Antibodies used for immunoblotting included the following: PSA (1:1000 dilution; cat# 5365S, Cell Signaling Technology), AR (1:1000 dilution, ab74272, Abcam), MTAP (1:1000 dilution, A20907, ABclonal), p-IRF3 (Ser396) (1:1000 dilution; MA5-14947, Themo Fisher), and γ-H2AX (1:1000 dilution; 9718, Cell Signaling Technology). Detailed information for all reagents used in this study were also provided in **Supplementary Materials**.

Analysis of public datasets The Cancer Genome Atlas (TCGA) Prostate Adenocarcinoma (TCGA-PRAD) and SU2C/PCF Dream Team datasets were retrieved from the cBioPortal (http://www.cbioportal.org/) for Cancer Genomics. According to the above datasets, comparative expression and survival analysis were performed with cBioPortal, Gene Expression Profiling Interactive Analysis (GEPIA) and Prostate Cancer Transcriptome Atlas (PCTA) bioinformatic tools.

In vitro cell growth assays In vitro cell growth assays were performed following previously described procedure[22,43]. Briefly, adherent cells were plated onto a 96-well plate at ~5% confluency with at least 3 biological replicates. Cell growth was monitored and quantified by confluency using the IncuCyte S3 Live-Cell Analysis system (Sartorius, Göttingen, Germany) with nine images per well taken with a 20x or 4x objective. The change in confluency was normalized to the confluency at Day 0. All cell growth assays were repeated in at least two independent experiments.

Metabolite profiling C4-2/MDVR metabolite profiling data was retrieved from our previous study [22]. Metabolite profiling of C4-2 and PC3 was performed following previously described procedures [22]. Briefly, cells were plated into six-well plates at 35% confluency with 3 technical replicates and treated with DMSO (vehicle), 5 μM DRP-104, 6 μM MTDIA, and 5 μM DRP-104 plus 6 μM MTDIA for 48 hours. The confluency of each of the wells was measured by the IncuCyte S3 Live-Cell Analysis system (Sartorius) before metabolite isolation. Cellular metabolites were extracted, as in our previous study [22,44]. Cells were collected in 80% methanol to extract the metabolites. After centrifugation, the supernatant was dried with a speed vacuum, and dry pellets were reconstituted into 30μL of sample solvent (water: methanol: acetonitrile, 2:1:1), followed by centrifugation at 20,000g for 3 minutes. The supernatant was transferred to LC vials, and 3 μL was submitted to be analyzed with high-performance liquid chromatography- high-resolution mass spectrometry (LC-MS) using previously described procedures [22,44].

Immunofluorescent staining and imaging for purinosome detection pFGAMS-EGFP plasmid was a gift from Dr. Stephen Benkovic (obtained from Addgene, plasmid# 99107) [40]. For purinosome detection, cells

($2*10^4$ per well) were plated on μ-Slide 4 well chambered coverslip (Ibidi, # 80426, Gräfelfing, Germany) and allowed to attached one day before the transfection. Then, cells were transiently transfected with plasmid pFGAMS-EGFP using Lipofectamine 3000 (Invitrogen, L3000015, ThermoFisher) according to the manufacturer's instructions. When pertinent, at the time of transfection cells were also transiently treated with agents such as DRP-104, Docetaxel or MTDIA. Two days later after the transfection, cells were washed with PBS, fixed in 4% formaldehyde (Santa Cruz Biotechnology, sc-281692, Dallas, TX, USA) at room temperature for 15 minutes, and permeabilized with 0.2% Triton X-100 (Bio-Rad, # 1610407, Hercules, CA, USA) for 15 minutes. They were then washed and stained with 1 µg/mL DAPI (MilliporeSigma, # D9542, Darmstadt, Germany) before the slides were mounted with ProLong Gold Antifade Mountant (ThermoFisher, # P36394). The slides were imaged with Zeiss 880 Airyscan Fast Inverted Confocal Microscope and analyzed using the Zeiss Zen 3.9 (blue edition) software (Carl Zeiss Microscopy GmbH, Oberkochen, Germany).

For endogenous PAICS immunofluorescent staining, cells were plated and treated as the above procedures without transfection. After 3 days of treatment, cells were washed with PBS, fixed in 4% formaldehyde (Santa Cruz Biotechnology) at room temperature for 15 minutes, and permeabilized with 0.2% Triton X-100 (Bio-Rad) for 15 minutes. Slides with fixed and permeabilized cells were blocked with blocking buffer (1% BSA, 0.2% Triton X-100, 10% goat serum, 0.2 M glycine in PBS) at room temperature for 1 hour, and then incubated with primary antibody (anti-PAICS, 12967-1-AP, Proteintech, Rosemont, IL, USA) diluted in antibody dilution buffer (1% BSA, 0.2% Triton X-100 in PBS; 1:200 dilution) at 4 °C overnight. The next day, slides were washed three times with PBS and incubated with the secondary antibody (anti-rabbit Alexa 594, A-11037, ThermoFisher) 1:500 diluted in antibody dilution buffer at room temperature for 1 hour. Then, cells were washed and stained with 1 µg/mL DAPI (MilliporeSigma) before the slides were mounted with ProLong Gold Antifade Mountant (ThermoFisher). The slides were imaged with Zeiss 880 Airyscan Fast Inverted Confocal Microscope and analyzed using the Zeiss Zen 3.9 (blue edition) software (Carl Zeiss Microscopy GmbH).

CRISPR-mediated gene knockout The *MTAP* knockout plasmid was constructed using pLentiCRISPR-E backbone (# 78852, Addgene). The sgRNA sequences for targeting the exon of *MTAP* was designed using the CRISPR program (http://crispor.tefor.net) and described previously (*MTAP* sgRNA sequence #1: GGCTCATCTCACCTTCACGG and sequence #2: CGTTTTAGCTCCCGGGCAGAC; Random control sequence #1: CAGCCACCGCACCGGCGTAA and sequence #2: ATGTTGCAGTTCGGCTCGAT)[45]. In brief, the paired sgRNA were first phosphorylated and annealed using T4 polynucleotide kinase (# M0201S, NEB), followed by ligation with the purified, linearized LentiCRISPRv2E vector (pre-digested with the restriction enzyme BsmBI) using T4 DNA ligase (# M0202S, NEB). Recombinant plasmids were verified to contain expected sgRNA sequences via colony PCR, using LKO.1 5' and pLentiCRISPR-R1/antisense primers). The *MTAP* CRISPR/Cas9 knockout lentivirus was produced by transfecting HEK293T cells with TransIT-X2® Dynamic Delivery System (# MIR 6004, Mirus Bio) and plasmids including pMD2.G, psPAX2, and two recombinant plasmids at a ratio of 3:4:6. Control lentivirus was prepared in parallel using LentiCRISPRv2E plasmids ligated with the random sequences. *MTAP* and control knockout in vitro model was generated by transducing C4-2 cell lines with lentivirus at a multiplicity of infection (MOI) of 1–2 in a laminin-coated 6-well plate. After 24 hours, the virus-containing medium was replaced with fresh RPMI1640 (CCF). The transduced cells were then selected with puromycin (# P8833; Millipore Sigma) at 1 µg/mL for several days until all non-transduced cells were eliminated. The surviving cells were subsequently maintained in 0.5 µg/mL puromycin. The successful knockout of *MTAP* was confirmed by anti-MTAP immunoblots.

Protein extraction and immunoblotting The cell pellet was washed once with pre-chilled PBS and lysed on ice for 30 minutes using RIPA lysis buffer (# R0278; Sigma-Aldrich) supplemented with phosphatase and protease inhibitors (# 1861281; Thermo Fisher). The lysate was sonicated on ice-water bath five times, then centrifuged at 12,000 rpm for 15 minutes at 4°C. The supernatant was collected and mixed with loading buffer (# 161074; Bio-Rad). The mixture was heated at 95-100°C for 5–7 minutes and then loaded onto an SDS-polyacrylamide gel (SDS-PAGE) for electrophoresis, followed by transfer onto an Immun-Blot PVDF membrane (# 1620177; Bio-Rad). The membrane was blocked in TBST containing 5% non-fat milk for 1 hour and then incubated with the primary antibody at 4°C on a shaker for 12–16 hours. After four washes with TBST, the membrane was incubated with an HRP-conjugated secondary antibody diluted at 1:7,000-1:10,000 at room temperature for 1 hour. Following another four washes with TBST, protein detection was performed using SuperSignal West Femto Maximum Sensitivity Substrate (# 34095; Thermo Fisher) and visualized using the iBright Imager (Thermo Fisher) software. Edited whole gel images are available upon request.

Reverse transcription-quantitative PCR Total RNA was extracted from the cell pellet using an RNA extraction kit (Cat# R1055; ZYMO RESEARCH) following the manufacturer’s instructions. The RNA concentration and absorbance were measured using a Nanodrop 2000 (Thermo Fisher). RNA samples with a concentration exceeding 50 ng/µL and an A260/A280 ratio above 1.9 were used for reverse transcription to synthesize cDNA (Cat# 4368814; Thermo Fisher). SYBR Green qPCR Master Mix (Cat# 11184ES08; YEASEN) and corresponding primers (Supplementary Materials) were mixed and added to each reaction well, with each target gene analyzed in duplicate. Real-time quantitative PCR (qPCR) was performed on a QuantStudio 3 instrument (Thermo Fisher). The housekeeping gene Actb/ACTB was used for normalization, and the relative expression of target genes was calculated using the $2^{\wedge-\Delta\Delta CT}$ method. Primers used for PCR were described in the Supplementary Materials.

ISRE-GFP reporter gene assays An ISRE-GFP reporter model was established by transducing target cells with lentivirus (Cat# LVP937-P, GenTarget) at a multiplicity of infection (MOI) of 1–2 in the presence of 4 µg/mL polybrene. After 12–24 hours, the culture medium was replaced with fresh DMEM to remove the residual virus. The infected cells were selected using 1 µg/mL puromycin (Cat# P8833; Millipore Sigma) until all uninfected cells died. The selected cells were maintained in the culture medium containing 0.5 µg/mL puromycin. The purified target cells were seeded at a density of 2%-3% in a 96-well plate, and compounds were added according to the experimental protocol. The cells were placed in an IncuCyte system for real-time monitoring, with scheduled daily scans to record the GFP signal area, mean fluorescence intensity, and cell confluency in each well. The total integrated GFP signal intensity (GCU μM^2/image) was calculated as the mean signal intensity × signal area/cell confluency. The relative increase in GFP signal was first calculated compared to day 0 and then normalized to the control group to quantify differences in ISRE pathway activation across treatment groups. Representative images were downloaded from the IncuCyte system.

In vivo tumor models and treatments The animal study was approved by the Institutional Animal Care and Use Committee (IACUC) of Duke University (A055-22-03). All mice were purchased from the Jackson Laboratory. For TrampC2-derived tumor modes, 24 immune-competent (wild-type), 6-8 week-old C57BL/6J mice were used. The subcutaneous inoculation was performed by injecting 0.5 million cells in PBS and Matrigel (Corning) mixture (1:1) under the right flank skin using a 27 ½ gauge syringe. This injection was performed under brief isoflurane anesthesia on a shaved ~1 cm^2 region of the flank. When the tumors reached approximately 100 mm^3, mice were randomized into six mice per group and treated three times per week, via subcutaneous (s.c.) and intraperitoneal (i.p.) injection for following treatments: (1) Tween 80: Ethanol: Saline (5:5:90) vehicle (s.c. injection) and corn oil vehicle (i.p. injection); (2) Tween 80: Ethanol: Saline (5:5:90) vehicle (s.c. injection) and 5 mg/kg MTDIA (MedKoo Bioscience, 407244, Durham, NC, USA) (i.p. injection); (3) 2 mg/kg DRP-104 (s.c. injection) and corn oil vehicle (i.p. injection), or (4) 2 mg/kg DRP-104 (s.c. injection) and 5 mg/kg MTDIA (i.p. injection). Body weight and xenograft size were measured 3 times a week with calipers by the same scientist throughout the experiment and calculated using tumor volume = $\text{length}*(\text{width})^2*0.5$ formula. Mice were sacrificed at 14 days of treatment because the control tumor size met humane end-stage criteria. Syngeneic tumors were dissected and tumor weight/volume was measured. For PC3-derived xenografts and treatments, 24 NSG mice were injected in the right flank with one million PC3 cells in culture media and Matrigel (Corning, 354234, Glendale, AZ, USA) mixture (1:1). Treatments and tumor monitoring were carried out following procedures that were used for the TrampC2 model.

Hematoxylin and eosin (H&E) staining and immunohistochemical staining H&E stains and immunohistochemical stains (IHC) were performed following standard procedures as we previously described [21,43]. Formalin-fixed paraffin-embedded (FFPE) sections at 4-5 mm were deparaffinized and rehydrated. Heat-mediated antigen retrieval was performed in a boiled water bath for 40 minutes in citrate buffer (pH 6.0). Antibodies were incubated at 4 °C overnight. Next day, slides were incubated for 45 minutes at room temperature with HRP-conjugated secondary antibodies (Dako Envision+Kit) and visualized with DAB.

Quantification and statistical analysis For quantification of purinosome, cell images were thresholded, and cells with FGAMS or PAICS granules were counted. For each biological repeat, at least 21 cells (for the quantification of FGAMS-EGFP granules, only transfected cells were counted) were analyzed in each group and the percentage of puncta positivity was quantified. Statistical analyses were performed by GraphPad

Prism 9. The unpaired two-tailed t-test was used for comparison between two groups, whereas one-way or two-way ANOVA was used for multigroup comparisons.

Results

Cancer cells under purine shortage stress reprogram their purine biosynthesis machinery as an adaptive response

Purines provide essential building blocks and serve as energy sources that cancer cells rely on for proliferation. Consequently, purine biosynthesis, particularly the de novo pathway, has been explored as a therapeutic target for treating various cancers, such as pancreatic and brain cancers [33,45-47]. Purine shortage can be induced by certain anti-cancer drugs, such as Methotrexate, an inhibitor of dihydrofolate reductase (DHFR), although toxicity remains a major limitation [34]. The recently developed, well-tolerated, clinical-grade prodrug of the broad-acting glutamine antagonist DON, known as DRP-104 (Sirpiglenastat), has shown excellent efficacy in several preclinical cancer models including PCa, and its direct suppressive effects on tumor cells are accompanied by the disruption of purine biosynthesis [8-10,22]. These findings suggest the feasibility of exploring this well-tolerated prodrug as an effective purine supply-blocking agent for cancer treatment.

Several additional lines of evidence further support this feasibility. First, DON (i.e., DRP-104) inhibits at least 10 enzymes in seven glutamine-utilizing metabolic pathways, with a wide range of potencies (Ki values from ~µMs to ~mMs) [23-32]. Notably, it inhibits FGAMS, an enzyme in the purine synthesis pathway, with the lowest Ki (~1.1 µM) [23-32], suggesting that purine biosynthesis is likely among the pathways most susceptible to DRP-104 (**Supplementary Fig. 1A-B**). Additionally, unbiased metabolic profiling in PCa cell lines PC3 and C4-2 demonstrated that purines were among the most affected metabolites following DRP-104 treatment (**Fig. 1A, Supplementary Fig. 2**). Importantly, supplementation with exogenous purines rescued cancer cells from the suppressive effects of DRP-104 (or DON); and this rescue effect was not unique to PCa cells, as it was also observed in NCI-H358, a lung cancer cell line (**Fig. 1B, Supplementary Fig. 3A**). Gene Set Enrichment Analysis (GSEA) of publicly available gene expression data [48] confirmed that the purine biosynthesis pathway is significantly upregulated during PCa pathogenesis **(Supplementary Fig. 3B-C)**. Finally, higher expression of FGAMS-encoding PFAS gene or the set of six genes encoding core enzymes of the purine biosynthesis machinery, namely purinosomes[36], was correlated with worse survival in PCa patients **(Supplementary Fig. 3D-F)**, providing further rationale for targeting purine supply as a therapeutic strategy.

While DRP-104 effectively suppresses tumor cell proliferation, it is unlikely to completely deplete purines from tumor cells. Instead, it is more feasible to induce a state of purine shortage. Over time, cells that survive this purine shortage may adapt to the stress and ultimately resume propagation, as observed with many targeted therapies. This hypothesis is supported by the observation that while DRP-104 or DON (typically in the range of 2-4 µM) effectively suppressed tumor cell proliferation, the treatment did not eradicate tumor cells. Eventually, the cells adapted to this stress and resumed growth, leading to the emergence of DRP-104-adaptive (resistant) cell lines capable of proliferating in the presence of DRP-104 (**Fig. 1C**, **Supplementary Fig. 4**). Although DRP-104-adaptive PC3 cells exhibited substantially slower growth compared to their DRP-104-naïve (parental) counterparts, DRP-104-adaptive C4-2 cells propagated at a rate similar to that of their treatment-naïve counterparts (**Fig. 1C**, **Supplementary Fig. 4**). We thus utilized the C4-2 models to investigate the mechanisms underlying the adaptation. Since C4-2 cells are AR-dependent and respond to AR inhibition, we first evaluated the response of these purine shortage-adaptive derivatives to the AR antagonist enzalutamide. These cells retained their susceptibility to the AR signaling blockade (**Fig. 1C-D**, **Supplementary Fig. 4**), consistent with the expectation that purine dependency is not exclusive to AR-driven cell proliferation. This also suggests that prior DRP-104 exposure does not interfere with the effectiveness of subsequent AR-targeting therapies. Most notably, we found that, compared to their DRP-104 naïve counterparts, DRP-104-adaptive cells displayed increased sensitivity to Docetaxel (**Fig. 1E**), a microtubule-stabilizing chemotherapeutic drug commonly used for advanced and metastatic PCa [49-54].

Microtubules, as key components of the cellular cytoskeleton, play essential roles in various cellular processes. In the context of cancer treatments, the focus has traditionally been on their roles in cell division, while other cellular processes have received less attention. One such underexplored process is purine biosynthesis in mammalian cells under purine shortage stress. In response to this stress, cells assemble multiple-subunit macromolecular complexes of de novo purine biosynthesis enzymes, known as purinosomes, as an adaptive mechanism to more efficiently ramp up purine biosynthesis[35-40]. Microtubules are essential for the assembly and proper spatial distribution of purinosomes, as demonstrated in previous studies[36,39,55-57]. Several lines of evidence suggest that the heightened sensitivity of DRP-104-resistant cells to Docetaxel, a microtubule-targeting drug, is due to their reprogrammed purine biosynthesis machinery and acquired dependency on purinosomes. First, using EGFP-tagged FGAMS, a well-established marker for purinosome detection [35-40], we observed a significant increase in purinosome-resembling foci in the resistant/adaptive cells, implicating purinosomes in enabling PCa cell resistance and adaptation (**Fig. 1F**). Secondly, treatment with Docetaxel - at doses that did not affect overall cell proliferation or survival – led to a reduction in purinosome abundance in the resistant cells, consistent with the drug's microtubule-targeting effects (**Fig. 1G**). Additionally, exogenous purine supplementation protected the resistant cells from the suppressive effects of Docetaxel (**Fig. H**), further underscoring the link between purinosome dependency and drug sensitivity.

Further supporting the role of DRP-104 as an inducer of purine shortage - and consistent with the findings from the DRP-104-adaptive cells described above - subsequent experiments confirmed that transient DRP-104 treatment effectively induces the formation of purinosomes across multiple cancer cell lines, including PCa cell lines (e.g., PC3 and C4-2), a lung cancer cell line (NCI-H358), and a mouse glioma cell line CT-2A (**Fig. 2A-B**). Results from the exogenously expressed EGFP-FGAMS-based purinosome detection were further validated by immunofluorescent staining targeting endogenous PAICS, another key enzyme in the de novo purine biosynthesis pathway and a commonly used marker for purinosome assays [35-40] (**Fig. 2C-D**).

Collectively, these results suggest that cancer cells under purine shortage stress reprogram their purine biosynthesis machinery – particularly through the microtubule-mediated assembly of purinosomes – as an adaptive mechanism.

MTAP-dependent purine salvage serves as a critical source of purine supply in cancer cells

Purine biosynthesis comprises two primary pathways: de novo biosynthesis and the salvage process. In the purine salvage pathway, MTAP converts 5′-methylthioadenosine (MTA), a byproduct of the polyamine biosynthesis pathway, into methionine and adenine. The adenine is subsequently converted by Adenine Phosphoribosyltransferase (APRT) to form AMP **(Supplementary Fig. 1B)**. Understanding the role of MTAP-mediated purine salvage in PCa cells' response to DRP-104 is critical. While MTAP alterations are prevalent in some cancer types, such as glioblastoma where approximately half of all tumors harbor homozygous MTAP loss, they present as various types of alterations in PCa and occur in only ~2-3% of cases (**Supplementary Fig. 5A**). Previous studies have investigated MTAP inhibition as a strategy to suppress multiple cancer types [58-60]. Inhibition of MTAP has been shown to directly suppress PCa cells [61], and that its inhibition along with stimulation of polyamine biosynthesis exacerbates the stress of one-carbon unit loss, thereby suppressing PCa progression[62]. However, the extent to which MTAP-dependent purine salvage contributes to purine supply in PCa remains unclear, especially in the context of cellular adaptation to purine shortage. To address this, PCa cells were treated with MTDIA, a specific transition state analogue inhibitor of MTAP [58-60], followed by unbiased metabolic profiling analysis. The results demonstrated that MTAP inhibition predominantly affected purine metabolism (**Fig. 3A**). Further, treating prostate cancer cell lines (C4-2, PC3) and the lung cancer cell line NCI-H358 with MTDIA resulted in an increased presence of purinosomes (**Fig. 3B-C, Supplementary Fig. 5B**), indicating that MTAP inhibition induces purine shortage stress. Additional experiments using CT-2A cell line models, including an *Mtap*-null derivative line[42], revealed a higher abundance of purinosomes in parental (*Mtap*-intact) CT-2A cells treated with MTDIA and in *Mtap*-null CT-2A cells compared to their parental, vehicle-treated counterparts (**Fig. 3D-E, Supplementary Fig. 5C**).

While it is generally believed that tumor cells primarily rely on *de novo* purine biosynthesis while also recycling purine precursors from the microenvironment [63], the results presented here suggest that cancer cells, even when cultured under standard conditions, sense purine shortage upon loss of MTAP function. Intriguingly, despite the clear role of MTAP-dependent purine salvage as a source of purine supply, cancer cell proliferation was not affected by MTAP inhibition, as shown in previous findings in glioma models [45], as well as in prostate cancer models described here (**Supplementary Fig. 5D**). In contrast, cancer cells adaptive to DRP-104 displayed measurable susceptibility to MTAP inhibition (**Supplementary Fig. 5D**).

The increased abundance of purinosomes, which are capable of more efficient de novo purine biosynthesis[35], in the MTAP-deficient cells led us to hypothesize that forming purinosomes is a way for tumor cells to compensate for the loss of purine salvage. In agreement with this hypothesis, we found that treating cancer cells with MTDIA in the presence of Docetaxel, at a dose that did not affect cell proliferation (**Fig. 3G**), resulted in significant suppression of proliferation (**Fig. 3H**). Most remarkably, similar treatment experiments in DRP-104-adaptive cells, which were more susceptible to Docetaxel compared to their naïve counterparts (as shown in **Fig. 1E,** and again comparing **Fig. 3J** versus **3G**), showed that compared to their naïve counterparts, these cells were also more sensitive to MTDIA (**Fig. 3** versus **3FI**), and displayed even higher susceptibility to the combinational treatment of MTDIA plus Docetaxel (**Fig. 3K** versus **3H**).

Collectively, these results suggest that MTAP inhibition triggers adaptive stress responses in cancer cells, marked by purinosome formation, thus underscoring the critical role of MTAP-dependent purine salvage as a consequential source of purine supply for cancer cells. Additionally, these findings corroborate the previously proposed critical roles of microtubule-mediated formation of purinosomes and suggest a functional link between MTAP and microtubules in the context of purine supply and shortage. Upon the loss of MTAP-mediated purine salvage, tumor cells resort to microtubules to assemble purinosomes (for more efficient purine biosynthesis as a compensatory adaptation), and vice versa. These two compensatory mechanisms of purine supply together become essential for enabling tumor cells to adapt to compromised de novo purine biosynthesis, as in the case of DRP-104 treatment.

Inhibiting MTAP sensitizes tumor cells to DRP-104 treatments

Several studies have investigated MTAP inhibition as a cancer treatment strategy using MTDIA, an orally bioavailable, potent, and specific transition state analogue inhibitor of MTAP [58-62]. The feasibility of therapeutically targeting MTAP, along with the compensatory relationship between MTAP-dependent purine salvage and de novo purine biosynthesis described above, led us to test the hypothesis that (1) MTAP-mediated purine salvage protects cancer cells from DRP-104-induced purine shortage and (2) inhibiting MTAP can enhance the tumor-suppressive effect of this prodrug.

First, we treated PCa cell lines with DRP-104 in the presence of exogenous MTAP substrate, 5'-deoxyadenosine (5’dAdo), and observed that 5’dAdo mitigated DRP-104-induced suppression of cell growth (**Fig. 4A, Supplementary Fig. 6A**). This finding suggests that although the strength of the purine salvage pathway may vary across cancer cell lines, excess MTAP substrate is protective. In contrast, the presence of MTAP inhibitor MTDIA potentiated the suppressive effects of DRP-104 (**Fig. 4B, Supplementary Fig. 6B**). We confirmed that the protective and damaging effects of 5'dAdo and MTDIA, respectively, were not due to their influence on the conversion of the prodrug, as similar effects were observed when using DON (**Fig. 4C**). To further corroborate these findings, we compared the metabolic profiles in C4-2 cell lines treated with DRP-104 plus MTDIA to those of the cells that were treated with DRP-104 alone. This analysis revealed that the combination treatment primarily affected purine metabolism, along with cysteine and methionine metabolism pathways, consistent with MTDIA-induced disruption of the purine supply (**Supplementary Fig. 6C-D, Supplementary Table 1**). As expected, purinosomes were prominently present in tumor cells that were treated with DRP-104 plus MTDIA, confirming both the occurrence of purine shortage in these cells and the enhanced suppressive effect of the DRP-104 and MTDIA combination (**Supplementary Fig. 6E**).

Furthermore, as a complementary strategy to the chemical approach (i.e., the use of MTDIA), we generated *MTAP*-null derivative cell line from C4-2 using CRISPR-mediated *MTAP* knockout (**Fig. 4D**) and confirmed that the *MTAP*-null cell line was more susceptible to DRP-104 or DON compared to the MTAP-intact controls (**Fig. 4E**). To assess whether MTDIA's ability to enhance DRP-104 efficacy extends beyond PCa, we tested DRP-104 sensitivity in NCI-H358, a lung cancer cell line. As observed in prostate cancer cell lines, MTDIA alone did not affect cell propagation but increased NCI-H358 cells' susceptibility to DRP-104 (**Supplementary Fig. 6F**). We further tested a previously described *Mtap*-null cell line derived from mouse glioma cell line CT-2A[42], and confirmed its increased susceptibility to DRP-104 (or DON) compared to its *Mtap*-intact counterpart (**Fig. 4F**). The role of Mtap in modulating tumor cell susceptibility to purine shortage – induced by treatments such as DRP-104 or DON - was also observed in another glioma cell line, GL261, using both chemical (MTDIA) and genetic (*Mtap* knockout) approaches (**Supplementary Fig. 6G-H**).

Collectively, these findings underscore the protective effects of MTAP-mediated purine salvage in purine shortage induced by DRP-104 therapy. They suggest that *MTAP* status should be a consideration when designing purine blockade-based treatments, and highlight the potential of MTAP inhibitors, such as MTDIA, to enhance the efficacy of purine shortage inducers such as DRP-104 in *MTAP*-intact cancers.

Combining DRP-104 with MTDIA yields superior therapeutic efficacy in a prostate cancer model in vivo

We next evaluated the therapeutic effects of simultaneous targeting MTAP and de novo purine biosynthesis by combining MTDIA and DRP-104 in vivo. In addition to directly suppressing tumor cells, DRP-104 has been shown to enhance anti-cancer immunity across several cancer types [10-12]. Notably, previous studies suggested that in certain cancers, such as pancreatic cancer and glioma, *MTAP* loss and the resulting accumulation of its substrate, methylthioadenosine (MTA), contribute to an immunosuppressive tumor microenvironment [42,64].

These findings raise the possibility that while combining MTDIA with DRP-104 may enhance direct tumor cell suppression, as demonstrated in vitro, any potential immunosuppressive effects of MTDIA might counteract this therapeutic benefit.

To evaluate this possibility, we generated subcutaneous tumors from PCa cell line TrampC2 in immune-competent C57BL/6 host mice to test the effects of the combination treatment versus single-agent treatments. Our previous study showed that the regimen of 2 mg/kg daily DRP-104 treatment, five days per week, effectively suppressed NCI-H660-derived xenograft growth [22]. To evaluate the therapeutic efficacy of combining DRP-104 and MTDIA, we reduced the treatment frequency as follows: DRP-104 (2 mg/kg), MTDIA (5 mg/kg), or both (2 mg/kg and 5 mg/kg, respectively) were administered three times per week for a total of seven treatments and tumor progression was monitored (see **Supplementary Fig. 7A**). The experiment confirmed that DRP-104 alone had measurable efficacy as expected, while MTDIA alone had minimal effects, as assessed by tumor volume and weight (**Fig. 5A-C**). Remarkably, the combination of both agents resulted in superior tumor suppression (**Fig. 5A-C**), without significantly affecting the body weights of the recipient mice (**Supplementary Fig. 7B**). H&E staining revealed that while tumors from vehicle- and MTDIA-treated mice have sheets of viable tumor cells that were actively proliferating as reflected by frequent mitotic figures (**Fig. 5D**). In contrast, DRP-104-treated tumors had more sparse tumor cells, segregated by immune cells, fibrosis and tumor necrosis (**Fig. 5D**). Notably, residual tissue masses from mice treated with the DRP-104 and MTDIA combination were composed of immune cells and fibrosis without appreciable tumor cells (**Fig. 5D**).

We then performed immunohistochemical (IHC) assays for selected immune biomarkers, including T lymphocyte markers (CD3 and CD8α) and immune checkpoint markers (PD-1 and PD-L1), to evaluate the effects of the comprehensive purine blockade (i.e., combination of DRP-104 and MTDIA) on the tumor immune microenvironment. These IHC assays revealed that vehicle-treated and MTDIA-treated tumors displayed minimal staining for CD3, CD8α, and PD-1 but high levels of PD-L1, indicating low T cell infiltration and an immunosuppressive tumor microenvironment (**Fig. 5E, Supplementary Fig. 7C**). In contrast, both DRP-104-treated and DRP-104 plus MTDIA-treated tumors showed robust staining for CD3 and CD8α, suggesting strong T cell infiltration (**Fig. 5E, Supplementary Fig. 7C**). Compared with vehicle-treated and MTDIA-treated tumors, DRP-104-treated tumors had significantly reduced PD-L1$^+$ cells and an increased presence of PD-1$^+$ cells, possibly indicating negative immunoregulatory feedback in tumors whose progression had been mitigated. Most notably, DRP-104 plus MTDIA-treated tumors showed a slight increase in PD-1$^+$ cells and were largely devoid of PD-L1$^+$ cells (**Fig. 5E, Supplementary Fig. 7C**), consistent with the histological observation that tumor cells were essentially all eradicated in tissues from the combination therapy group (**Fig. 5D**).

The above results suggest that the superior therapeutic efficacy of the combination therapy is likely due to two factors: more effective direct tumor cell-autonomous suppression and the reshaping of the tumor immune microenvironment to stimulate anti-tumor immunity. This implies that the combination therapy may enhance, rather than diminish, DRP-104-induced anti-tumor immunity. Additionally, the findings from the in vivo model further corroborate results from in vitro studies and highlight the potential of combining MTAP inhibitors, such as MTDIA, with DRP-104 to achieve superior therapeutic outcomes in cancers that retain functional MTAP.

Purine supply deficiency leads to activated cGAS-STING signal pathway

The DRP-104-induced changes in the tumor immune microenvironment prompted us to investigate the mechanisms underlying the effects of this tumor cell-specific prodrug. Several previous findings are particularly noteworthy. First, an abundant supply of purine is critical for tumor cells' response to DNA damage [65-67]. Additionally, a compromised DNA damage response is linked to the cytosolic double-stranded DNA-sensing cGAS-STING pathway and innate immunity[68]. Indeed, it has been shown that a deficiency in the DNA damage response in PCa activates the cGAS-STING pathway [69]. Given that the status of the cGAS-STING pathway is a key determinant of the PCa immune microenvironment [70], we assessed the link between DRP-104-induced purine shortage, DNA damage and the cGAS-STING pathway. Intriguingly, transient in vitro treatment with DRP-104 led to elevated levels of γH2AX and phosphorylated IRF3 (p-IRF3), a downstream mediator of the cGAS-STING signal (**Supplementary Fig. 8A**), along with increased expression of interferon response genes such as *Ifnb1* and *Ccl5* (**Supplementary Fig. 8B**). These findings suggest a connection between purine shortage, DNA damage, and activation of the cGAS-STING pathway. As the tissue masses remaining after the treatments were mostly depleted of cancer cells and infiltrated with immune cells in the immune-competent tumor models mentioned above, we sought to establish xenografts in immunocompromised mice to further investigate. Our recent study shows that prostate cancer, together with brain tumors, is among the cancer types where the *STING1* gene is most heavily epigenetically silenced [71]. Nevertheless, the cGAS-STING pathway remains intact and can be functionally activated in certain prostate cancer cell lines, including PC3 and C4-2[69]. We therefore generated PC3-derived xenografts and treated tumor-bearing immunocompromised mice following the regimens described above (**Supplementary Fig. 7A**). The results corroborated findings from the TrampC2 model, demonstrating the superior efficacy of combining DRP-104 and MTDIA compared to each monotherapy (**Fig 6A**). We harvested the treated tumors at their endpoints and performed H&E staining and IHC for Ki67 to confirm the presence of tumor cells (**Supplementary Fig. 8C**), consistent with the expected direct suppressive effects on tumor cells rather than robust tumor cell eradication through anti-tumor immunity. Most importantly, γH2AX and p-IRF3 IHC assays revealed that tumors treated with DRP-104 or combination therapy displayed elevated levels of both markers (**Fig. 6B-C**), supporting a connection between purine shortage, DNA damage, and the cGAS-STING pathway in vivo.

We further employed an ISRE (interferon-stimulated response element) reporter-based assay[72] to assess the effects of DRP-104 on the cGAS-STING pathway in PC3 cells in vitro. We found that carboplatin, a genotoxic drug that is used for treating CRPC or small cell carcinoma of the prostate, activated the reporter signal as expected, and notably, DRP-104 treatment similarly stimulated the reporter signal, albeit to a lesser degree (**Fig. 6D, Supplementary Fig. 8D**). Furthermore, both carboplatin and DRP-104-stimulated reporter expression were mitigated by H-151, a STING antagonist (**Fig. 6D, Supplementary Fig. 8D**). These findings from the reporter-based assays were corroborated in the C4-2 cell line (**Fig. 6E**). To test whether the DRP-104 and cGAS-STING link is present in other tumor models, we extended the assay to glioma cell line CT-2A, given that the critical roles of purine supply in DNA damage repair have been well established in gliomas[66,67]. We confirmed that purine shortage, induced by either DRP-104 (in the *Mtap*-null CT-2A derivative line) or DRP-104 plus MTDIA (in the parental, *Mtap*-intact CT-2A cells), similarly resulted in activation of the reporter signal (**Fig. 6F-G, Supplementary Fig. 8E-F**). Finally, we used *IFNB1* and *CCL5* as the ISRE-regulated marker genes and assessed their expression in response to the treatments. In PC3 cells, these genes had very low basal expression levels, leading to variable results. However, in C4-2 and in CT-2A models, the expression of these genes was consistently stimulated by DRP-104 treatments (**Fig. 6F-G, Supplementary Fig. 8G**).

Collectively, these results are consistent with the scenario in which purine shortage, such as treatment with DRP-104, leads to activation of the cGAS-STING signal pathway in tumor cells. While the contribution of this pathway's activation to alterations in the tumor immune microenvironment and adaptive anti-tumor immunity remains to be elucidated, these findings suggest that purine shortage stress compromises the immunoevasive capacity of tumor cells. They also offer a potential mechanistic explanation for the DRP-104-induced changes in the tumor immune microenvironment in the TrampC2 model described above, as well as in tumor models of several other cancer types [10-13]**.**

Discussion

In this study, we demonstrate that purine supply represents a major liability in cancer cells that can be exploited for therapeutic purpose. We show that purine shortage is a key mechanism underlying the tumor-suppressive effects of DRP-104 (i.e., DON), a glutamine antagonist, across several cancer cell models. This finding aligns with recent studies highlighting the critical roles of purine supply and its disruption in lung cancer models treated with DRP-104[12], suggesting that this purine shortage-centered mechanism of DRP-104 may be broadly applicable to many cancer types. Most importantly, our work illustrates cellular processes that enable cancer cells to adapt (i.e., develop resistance) to purine shortage and uncovers their vulnerabilities under such a stress. We reveal that cancer cells utilize microtubule-mediated assembly of purinosome-resembling complexes to sustain their purine supply during purine shortage, thereby identifying microtubules as a therapeutic vulnerability in tumor cells under such stress. Additionally, we establish MTAP-dependent purine salvage as a critical source of purine supply in tumor cells, including PCa, lung cancer and glioma cell lines, both under purine-rich conditions and, more notably, during purine shortage (e.g., following DRP-104 treatment). Our findings highlight a novel, protective role of this pathway in tumor cells stressed by DRP-104 treatment. This suggests that targeting the purine salvage pathway could enhance the effects of purine blockade-based therapies. We further demonstrate that purine shortage stress is linked to elevated levels of DNA damage and activation of the cytosolic double-stranded DNA-sensing cGAS-STING pathway, suggesting compromised immune evasion capacity in tumor cells and offering a potential explanation for the DRP-104-induced alterations in the tumor immune microenvironment. Together, these findings inform the mechanisms of DRP-104's action, the processes underlying tumor cell adaptation/resistance to purine shortage, and future efforts to devise efficacious purine blockade-based therapeutic strategies as described below.

First, while DRP-104 (i.e., DON) is expected to broadly inhibit multiple glutamine-related metabolic enzymes and pathways, its potency against these targets varies, as indicated by the wide range of the Ki values reported in previous studies [23-32]. Additionally, quantifying the extent to which inhibition of each pathway contributes to tumor-suppressive effects is a challenging task, which can be further compounded by variables such as inhibition kinetics (i.e., doses & timepoints), the strength and roles of specific metabolic pathways in tumor cells, and potential cellular compensation mechanisms. Despite these limitations, the results presented here provide multiple independent lines of evidence to support that purine biosynthesis is among the most consequential processes mediating tumor cell-autonomous suppressive effects of DRP-104 across various cancer types, including PCa, lung cancer and glioma cells. Together with recent findings from the *KEAP1* mutant lung cancer models[12], these results suggest that purine shortage is an essential mediator of DRP-104's effects on tumor cells from diverse tissues of origin. We speculate two non-mutually exclusive underlying mechanisms to explain this observation: (i) purine biosynthesis may be the pathway most sensitive to DON (i.e., DRP-104), and/or (ii) purine biosynthesis may hold particular importance for tumor cell propagation compared to other DON-targeted pathways. Further studies are warranted to assess the effects of purine blockade in different cancer types. Additionally, elucidating the interplays between the disruption of purine biosynthesis and glutamine-related metabolic pathways affected by DRP-104 treatment will further enhance our understanding of tumor cell's adaptation and inform the development of combination therapies.

Second, while the important roles of de novo purines biosynthesis in cancer cells has been well documented[73,74], recent findings suggest that tumor cells also recycle purines from microenvironment, including dietary sources, to meet their constant need of these essential metabolites[63]. Our findings uncover two new cellular processes that tumor cells employ to ensure sufficient purine supply under purine shortage stress: microtubule-mediated formation of purinosomes - macromolecular complexes composing of multiple de novo purine biosynthesis enzymes that enhance purine biosynthesis [35,36,39] - and MTAP-dependent purine salvage. The involvement of purinosomes in tumor cells' adaptive response to purine biosynthesis inhibition is particularly interesting for two reasons. First, it raises the possibility that these multienzyme complexes may also contribute to tumor progression beyond experimentally induced purine shortage, as highly purine-dependent tumor cells could utilize such complexes to efficiently produce purines to fuel their rapid proliferation. Second, the assembly and proper spatial distribution of purinosomes depend on microtubules and heat shock proteins (e.g., Hsp90 and Hsp70)[38,55,56]. Notably, both microtubules and heat shock proteins are established therapeutic targets in cancer, raising the question of whether drugs targeting these components, such as Docetaxel and Hsp90 inhibitors, might exert part of their anti-tumor effects by impairing purine biosynthesis efficiency, in addition to their known impacts on cell division and oncoprotein functionality. Supported by the effects of Docetaxel described in this study, we suggest that further investigations into this question are warranted, as the outcomes could have direct implications for stratifying cancer patient for specific treatments and understanding mechanisms of resistance to these therapies. For instance, tumors with high purine demand may be more susceptible to these therapies, and reprogramming of purine biosynthesis machinery could potentially underlie resistance to these treatments.

Genetic alterations of MTAP, mostly in the form of homozygous co-deletion with its neighboring tumor suppressor gene *CDKN2A*, are common events in a variety of human cancers [75,76]. These alterations have been shown to promote tumor progression and aggressiveness, while also suggesting the potential to exploit the resultant MTAP deficiency for treatments [42,45,47,77-79]. Intriguingly, *MTAP* alterations occur only in a small subset of PCa [75,76], supporting the speculation that MTAP may be pro-tumorigenic in prostate cancers[61]. Several previous studies have explored MTAP inhibition for suppressing multiple cancer types, including lung, colon, prostate, and head and neck cancers, by leveraging MTDIA, a potent and specific transition state analogue inhibitor of MTAP [58-61]. Results from this study suggest that MTAP-mediated purine salvage can serve as an important source of purine supply in prostate and other *MTAP*-intact cancer cells, particularly under conditions of purine shortage. While the roles of MTAP in methionine salvage and the polyamine pathway in PCa pathogenesis remain to be fully addressed, we speculate that MTAP may be pro-tumorigenic in certain contexts through its roles in purine salvage. This aligns with the idea of targeting the MTAP pathway for treating PCa [61]. Additionally, similar observations regarding MTAP's role as a purine supply source were made in models of PCa and gliomas. This further supports the idea of exploiting purine blockade to treat cancers with homozygous *MTAP* deletion (i.e., approximately 50% of glioblastomas)[45-47]. Notably, MTAP functions as a purine supply source in cancer types with vastly different frequencies of homozygous *MTAP* deletion; glioblastoma exhibits the highest frequency, while PCa is among the lowest [75,76]. It is possible that compared to PCa, glioblastoma cells more readily adapt to the loss of purine salvage and/or derive greater benefits from the immunosuppressive microenvironment that MTAP loss may create [42,64,80].

Finally, in addition to directly suppressing the propagation of tumor cells, DRP-104 exerts anti-cancer immunity in multiple tumor models in immunocompetent hosts [10-12]. Previous studies have suggested that MTAP loss contributes to immunosuppressive tumor microenvironment in certain solid tumors [42,64]. Our findings from in vitro and in vivo tumor models suggest that combination treatment - adding MTDIA to DRP-104 - likely induces equally strong, if not stronger, anti-tumor immunity compared to DRP-104 monotherapy. Most importantly, multiple lines of independent evidence from in vitro and in vivo models support that purine shortage is accompanied by elevated levels of DNA damages and activation of the cytosolic double-stranded DNA-sensing cGAS-STING pathway. Although the precise mechanisms linking these cellular processes remain to be fully elucidated, they offer a potential explanation for the effects of DRP-104 on the tumor immune microenvironment [10-13]. Mechanisms aside, the potential impact of purine shortage on cancer cells' DNA damage levels and immune evasion capability has significant therapeutic implications. For example, incorporating DRP-104 into genotoxic treatment regimens could enhance therapeutic efficacy while potentially reducing genotoxicity in normal tissues. Additionally, since the *STING1* gene is often epigenetically silenced in cancers, a process reversible by DNA methyltransferase (DNMT) inhibitors[71], it is plausible combining DRP-104 with DNMT inhibitors could potentiate anti-tumor effects.

In summary, while the detailed mechanisms underlying cancer cells' resilience and vulnerability to therapeutically induced purine shortage remain to be further characterized in diverse cellular contexts and in vivo models, we propose that further studies exploring the purine blockade approach in additional prostate cancer models and in other cancer types - including those that frequently harbor *MTAP* loss, such as glioblastoma and lung cancers - are warranted.

References

1 Wang, Y. *et al.* Coordinative metabolism of glutamine carbon and nitrogen in proliferating cancer cells under hypoxia. *Nature communications* **10**, 201 (2019). https://doi.org:10.1038/s41467-018-08033-9

2 Oizel, K. *et al.* Formate induces a metabolic switch in nucleotide and energy metabolism. *Cell Death Dis* **11**, 310 (2020). https://doi.org:10.1038/s41419-020-2523-z

3 Lane, A. N. & Fan, T. W. Regulation of mammalian nucleotide metabolism and biosynthesis. *Nucleic acids research* **43**, 2466-2485 (2015). https://doi.org:10.1093/nar/gkv047

4 Altman, B. J., Stine, Z. E. & Dang, C. V. From Krebs to clinic: glutamine metabolism to cancer therapy. *Nature reviews. Cancer* **16**, 619-634 (2016). https://doi.org:10.1038/nrc.2016.71

5 Kim, G. W. *et al.* Glutamine Synthetase as a Therapeutic Target for Cancer Treatment. *Int J Mol Sci* **22** (2021). https://doi.org:10.3390/ijms22041701

6 Xu, L. *et al.* Targeting glutamine metabolism network for the treatment of therapy-resistant prostate cancer. *Oncogene* **41**, 1140-1154 (2022). https://doi.org:10.1038/s41388-021-02155-z

7 Xu, L. *et al.* A glutaminase isoform switch drives therapeutic resistance and disease progression of prostate cancer. *Proceedings of the National Academy of Sciences of the United States of America* **118** (2021). https://doi.org:10.1073/pnas.2012748118

8 Lemberg, K. M., Vornov, J. J., Rais, R. & Slusher, B. S. We're Not "DON" Yet: Optimal Dosing and Prodrug Delivery of 6-Diazo-5-oxo-L-norleucine. *Molecular cancer therapeutics* **17**, 1824-1832 (2018). https://doi.org:10.1158/1535-7163.MCT-17-1148

9 Tenora, L. *et al.* Tumor-Targeted Delivery of 6-Diazo-5-oxo-l-norleucine (DON) Using Substituted Acetylated Lysine Prodrugs. *Journal of medicinal chemistry* **62**, 3524-3538 (2019). https://doi.org:10.1021/acs.jmedchem.8b02009

10 Rais, R. *et al.* Discovery of DRP-104, a tumor-targeted metabolic inhibitor prodrug. *Sci Adv* **8**, eabq5925 (2022). https://doi.org:10.1126/sciadv.abq5925

11 Yokoyama, Y., Estok, T. M. & Wild, R. Sirpiglenastat (DRP-104) Induces Antitumor Efficacy through Direct, Broad Antagonism of Glutamine Metabolism and Stimulation of the Innate and Adaptive Immune Systems. *Molecular cancer therapeutics* **21**, 1561-1572 (2022). https://doi.org:10.1158/1535-7163.MCT-22-0282

12 Pillai, R. *et al.* Glutamine antagonist DRP-104 suppresses tumor growth and enhances response to checkpoint blockade in KEAP1 mutant lung cancer. *Sci Adv* **10**, eadm9859 (2024). https://doi.org:10.1126/sciadv.adm9859

13 Encarnacion-Rosado, J. *et al.* Targeting pancreatic cancer metabolic dependencies through glutamine antagonism. *Nat Cancer* **5**, 85-99 (2024). https://doi.org:10.1038/s43018-023-00647-3

14 Swami, U., McFarland, T. R., Nussenzveig, R. & Agarwal, N. Advanced Prostate Cancer: Treatment Advances and Future Directions. *Trends Cancer* **6**, 702-715 (2020). https://doi.org:10.1016/j.trecan.2020.04.010

15 Smith, M. R. *et al.* Apalutamide Treatment and Metastasis-free Survival in Prostate Cancer. *N Engl J Med* **378**, 1408-1418 (2018). https://doi.org:10.1056/NEJMoa1715546

16 Hussain, M. *et al.* Enzalutamide in Men with Nonmetastatic, Castration-Resistant Prostate Cancer. *N Engl J Med* **378**, 2465-2474 (2018). https://doi.org:10.1056/NEJMoa1800536

17 de Bono, J. S. *et al.* Abiraterone and increased survival in metastatic prostate cancer. *N Engl J Med* **364**, 1995-2005 (2011). https://doi.org:10.1056/NEJMoa1014618

18 Beer, T. M. *et al.* Enzalutamide in metastatic prostate cancer before chemotherapy. *N Engl J Med* **371**, 424-433 (2014). https://doi.org:10.1056/NEJMoa1405095

19 Spetsieris, N., Boukovala, M., Patsakis, G., Alafis, I. & Efstathiou, E. Neuroendocrine and Aggressive-Variant Prostate Cancer. *Cancers (Basel)* **12** (2020). https://doi.org:10.3390/cancers12123792

20 Aggarwal, R. *et al.* Clinical and Genomic Characterization of Treatment-Emergent Small-Cell Neuroendocrine Prostate Cancer: A Multi-institutional Prospective Study. *Journal of clinical oncology : official journal of the American Society of Clinical Oncology* **36**, 2492-2503 (2018). https://doi.org:10.1200/JCO.2017.77.6880

21 Cheng, Q. *et al.* Pre-existing Castration-resistant Prostate Cancer-like Cells in Primary Prostate Cancer Promote Resistance to Hormonal Therapy. *Eur Urol* **81**, 446-455 (2022). https://doi.org:10.1016/j.eururo.2021.12.039

22 Moon, D. *et al.* Targeting glutamine dependence with DRP-104 inhibits proliferation and tumor growth of castration-resistant prostate cancer. *Prostate* **84**, 349-357 (2024). https://doi.org:10.1002/pros.24654

23 Kaufman, E. R. Isolation and characterization of a mutant Chinese hamster cell line resistant to the glutamine analog 6-diazo-5-oxo-L-norleucine. *Somat Cell Mol Genet* **11**, 1-10 (1985). https://doi.org:10.1007/BF01534729

24 Levenberg, B., Melnick, I. & Buchanan, J. M. Biosynthesis of the purines. XV. The effect of aza-L-serine and 6-diazo-5-oxo-L-norleucine on inosinic acid biosynthesis de novo. *The Journal of biological chemistry* **225**, 163-176 (1957).

25 Hartman, S. C. The Interaction of 6-Diazo-5-Oxo-L-Norleucine with Phosphoribosyl Pyrophosphate Amidotransferase. *The Journal of biological chemistry* **238**, 3036-3047 (1963).

26 Livingston, R. B., Venditti, J. M., Cooney, D. A. & Carter, S. K. Glutamine antagonists in chemotherapy. *Adv Pharmacol Chemother* **8**, 57-120 (1970). https://doi.org:10.1016/s1054-3589(08)60594-3

27 Levitzki, A., Stallcup, W. B. & Koshland, D. E., Jr. Half-of-the-sites reactivity and the conformational states of cytidine triphosphate synthetase. *Biochemistry* **10**, 3371-3378 (1971). https://doi.org:10.1021/bi00794a009

28 LaRonde-LeBlanc, N., Resto, M. & Gerratana, B. Regulation of active site coupling in glutamine-dependent NAD(+) synthetase. *Nature structural & molecular biology* **16**, 421-429 (2009). https://doi.org:10.1038/nsmb.1567

29 Thomas, A. G. *et al.* Kinetic characterization of ebselen, chelerythrine and apomorphine as glutaminase inhibitors. *Biochem Biophys Res Commun* **438**, 243-248 (2013). https://doi.org:10.1016/j.bbrc.2013.06.110

30 Jayaram, H. N., Cooney, D. A., Milman, H. A., Homan, E. R. & Rosenbluth, R. J. Don, conv and donv--I. Inhibition of L-asparagine synthetase in vitro. *Biochem Pharmacol* **25**, 1571-1582 (1976).

https://doi.org:10.1016/0006-2952(76)90466-4
31 Tiemeier, D. C. & Milman, G. Chinese hamster liver glutamine synthetase. Purification, physical and biochemical properties. *The Journal of biological chemistry* **247**, 2272-2277 (1972).
32 Walker, B. *et al.* Inhibition of Escherichia coli glucosamine synthetase by novel electrophilic analogues of glutamine--comparison with 6-diazo-5-oxo-norleucine. *Bioorg Med Chem Lett* **10**, 2795-2798 (2000). https://doi.org:10.1016/s0960-894x(00)00565-5
33 Mullen, N. J. & Singh, P. K. Nucleotide metabolism: a pan-cancer metabolic dependency. *Nature reviews. Cancer* **23**, 275-294 (2023). https://doi.org:10.1038/s41568-023-00557-7
34 Hamed, K. M. *et al.* Overview of Methotrexate Toxicity: A Comprehensive Literature Review. *Cureus* **14**, e29518 (2022). https://doi.org:10.7759/cureus.29518
35 Zhao, H. *et al.* Quantitative analysis of purine nucleotides indicates that purinosomes increase de novo purine biosynthesis. *The Journal of biological chemistry* **290**, 6705-6713 (2015). https://doi.org:10.1074/jbc.M114.628701
36 Pedley, A. M. & Benkovic, S. J. A New View into the Regulation of Purine Metabolism: The Purinosome. *Trends in biochemical sciences* **42**, 141-154 (2017). https://doi.org:10.1016/j.tibs.2016.09.009
37 Pareek, V., Tian, H., Winograd, N. & Benkovic, S. J. Metabolomics and mass spectrometry imaging reveal channeled de novo purine synthesis in cells. *Science* **368**, 283-290 (2020). https://doi.org:10.1126/science.aaz6465
38 French, J. B. *et al.* Hsp70/Hsp90 chaperone machinery is involved in the assembly of the purinosome. *Proceedings of the National Academy of Sciences of the United States of America* **110**, 2528-2533 (2013). https://doi.org:10.1073/pnas.1300173110
39 French, J. B. *et al.* Spatial colocalization and functional link of purinosomes with mitochondria. *Science* **351**, 733-737 (2016). https://doi.org:10.1126/science.aac6054
40 An, S., Kumar, R., Sheets, E. D. & Benkovic, S. J. Reversible compartmentalization of de novo purine biosynthetic complexes in living cells. *Science* **320**, 103-106 (2008). https://doi.org:10.1126/science.1152241
41 Parker, S. *et al.* Immunotoxin-alphaCD40 therapy activates innate and adaptive immunity and generates a durable antitumor response in glioblastoma models. *Science translational medicine* **15**, eabn5649 (2023). https://doi.org:10.1126/scitranslmed.abn5649
42 Hansen, L. J. *et al.* MTAP loss correlates with an immunosuppressive profile in GBM and its substrate MTA stimulates alternative macrophage polarization. *Scientific reports* **12**, 4183 (2022). https://doi.org:10.1038/s41598-022-07697-0
43 Hauck, J. S. *et al.* Heat shock factor 1 directly regulates transsulfuration pathway to promote prostate cancer proliferation and survival. *Commun Biol* **7**, 9 (2024). https://doi.org:10.1038/s42003-023-05727-9
44 Gao, X. *et al.* Serine Availability Influences Mitochondrial Dynamics and Function through Lipid Metabolism. *Cell Rep* **22**, 3507-3520 (2018). https://doi.org:10.1016/j.celrep.2018.03.017
45 Hansen, L. J. *et al.* MTAP Loss Promotes Stemness in Glioblastoma and Confers Unique Susceptibility to Purine Starvation. *Cancer Res* **79**, 3383-3394 (2019). https://doi.org:10.1158/0008-5472.CAN-18-1010
46 Singh, S. X. *et al.* Purine Synthesis Inhibitor L-Alanosine Impairs Mitochondrial Function and Stemness of Brain Tumor Initiating Cells. *Biomedicines* **10** (2022). https://doi.org:10.3390/biomedicines10040751
47 Hu, Q. *et al.* MTAP Deficiency-Induced Metabolic Reprogramming Creates a Vulnerability to Cotargeting De Novo Purine Synthesis and Glycolysis in Pancreatic Cancer. *Cancer Res* **81**, 4964-4980 (2021). https://doi.org:10.1158/0008-5472.CAN-20-0414
48 You, S. *et al.* Integrated Classification of Prostate Cancer Reveals a Novel Luminal Subtype with Poor Outcome. *Cancer Res* **76**, 4948-4958 (2016). https://doi.org:10.1158/0008-5472.CAN-16-0902
49 Petrylak, D. P. *et al.* Docetaxel and estramustine compared with mitoxantrone and prednisone for advanced refractory prostate cancer. *The New England journal of medicine* **351**, 1513-1520 (2004). https://doi.org:10.1056/NEJMoa041318
50 Berthold, D. R. *et al.* Docetaxel plus prednisone or mitoxantrone plus prednisone for advanced prostate cancer: updated survival in the TAX 327 study. *Journal of clinical oncology : official journal of the American Society of Clinical Oncology* **26**, 242-245 (2008). https://doi.org:10.1200/JCO.2007.12.4008

51 Tannock, I. F. *et al.* Docetaxel plus prednisone or mitoxantrone plus prednisone for advanced prostate cancer. *The New England journal of medicine* **351**, 1502-1512 (2004). https://doi.org:10.1056/NEJMoa040720

52 Clarke, N. W. *et al.* Addition of docetaxel to hormonal therapy in low- and high-burden metastatic hormone sensitive prostate cancer: long-term survival results from the STAMPEDE trial. *Annals of oncology : official journal of the European Society for Medical Oncology* **30**, 1992-2003 (2019). https://doi.org:10.1093/annonc/mdz396

53 Sweeney, C. J. *et al.* Chemohormonal Therapy in Metastatic Hormone-Sensitive Prostate Cancer. *The New England journal of medicine* **373**, 737-746 (2015). https://doi.org:10.1056/NEJMoa1503747

54 Mahal, B. A. *et al.* Mortality Risk for Docetaxel-Treated, High-Grade Prostate Cancer With Low PSA Levels: A Meta-Analysis. *JAMA Netw Open* **6**, e2340787 (2023). https://doi.org:10.1001/jamanetworkopen.2023.40787

55 An, S., Deng, Y., Tomsho, J. W., Kyoung, M. & Benkovic, S. J. Microtubule-assisted mechanism for functional metabolic macromolecular complex formation. *Proceedings of the National Academy of Sciences of the United States of America* **107**, 12872-12876 (2010). https://doi.org:10.1073/pnas.1008451107

56 Chan, C. Y. *et al.* Microtubule-directed transport of purine metabolons drives their cytosolic transit to mitochondria. *Proceedings of the National Academy of Sciences of the United States of America* **115**, 13009-13014 (2018). https://doi.org:10.1073/pnas.1814042115

57 Sha, Z. & Benkovic, S. J. Purinosomes spatially co-localize with mitochondrial transporters. *The Journal of biological chemistry* **300**, 107620 (2024). https://doi.org:10.1016/j.jbc.2024.107620

58 Basu, I. *et al.* Growth and metastases of human lung cancer are inhibited in mouse xenografts by a transition state analogue of 5'-methylthioadenosine phosphorylase. *The Journal of biological chemistry* **286**, 4902-4911 (2011). https://doi.org:10.1074/jbc.M110.198374

59 Firestone, R. S. *et al.* Transition state analogue of MTAP extends lifespan of APC(Min/+) mice. *Scientific reports* **11**, 8844 (2021). https://doi.org:10.1038/s41598-021-87734-6

60 Basu, I. *et al.* A transition state analogue of 5'-methylthioadenosine phosphorylase induces apoptosis in head and neck cancers. *The Journal of biological chemistry* **282**, 21477-21486 (2007). https://doi.org:10.1074/jbc.M702287200

61 Bistulfi, G. *et al.* The essential role of methylthioadenosine phosphorylase in prostate cancer. *Oncotarget* **7**, 14380-14393 (2016). https://doi.org:10.18632/oncotarget.7486

62 Affronti, H. C. *et al.* Pharmacological polyamine catabolism upregulation with methionine salvage pathway inhibition as an effective prostate cancer therapy. *Nature communications* **11**, 52 (2020). https://doi.org:10.1038/s41467-019-13950-4

63 Tran, D. H. *et al.* De novo and salvage purine synthesis pathways across tissues and tumors. *Cell* **187**, 3602-3618 e3620 (2024). https://doi.org:10.1016/j.cell.2024.05.011

64 Gjuka, D. *et al.* Enzyme-mediated depletion of methylthioadenosine restores T cell function in MTAP-deficient tumors and reverses immunotherapy resistance. *Cancer cell* **41**, 1774-1787 e1779 (2023). https://doi.org:10.1016/j.ccell.2023.09.005

65 Qi, S. *et al.* Electrochemical response mechanism of DNA damaged cells: DNA damage repair and purine metabolism activation. *Bioelectrochemistry* **161**, 108832 (2025). https://doi.org:10.1016/j.bioelechem.2024.108832

66 Zhou, W. *et al.* Purine metabolism regulates DNA repair and therapy resistance in glioblastoma. *Nature communications* **11**, 3811 (2020). https://doi.org:10.1038/s41467-020-17512-x

67 Zhou, W. & Wahl, D. R. Purine metabolism promotes radioresistance and is a therapeutic target in glioblastoma. *Mol Cell Oncol* **7**, 1834902 (2020). https://doi.org:10.1080/23723556.2020.1834902

68 Li, T. & Chen, Z. J. The cGAS-cGAMP-STING pathway connects DNA damage to inflammation, senescence, and cancer. *The Journal of experimental medicine* **215**, 1287-1299 (2018). https://doi.org:10.1084/jem.20180139

69 Tang, Z. *et al.* ATR Inhibition Induces CDK1-SPOP Signaling and Enhances Anti-PD-L1 Cytotoxicity in Prostate Cancer. *Clinical cancer research : an official journal of the American Association for Cancer Research* **27**, 4898-4909 (2021). https://doi.org:10.1158/1078-0432.CCR-21-1010

70 Zhuo, X., Dai, H. & Yu, S. The cGAS-STING pathway-related gene signature can predict patient prognosis and immunotherapy responses in prostate adenocarcinoma. *Medicine (Baltimore)* **101**,

e31290 (2022). https://doi.org:10.1097/MD.0000000000031290

71 Low, J. T. *et al.* Epigenetic STING silencing is developmentally conserved in gliomas and can be rescued by methyltransferase inhibition. *Cancer cell* **40**, 439-440 (2022). https://doi.org:10.1016/j.ccell.2022.04.009

72 Barnett, K. C. *et al.* Phosphoinositide Interactions Position cGAS at the Plasma Membrane to Ensure Efficient Distinction between Self- and Viral DNA. *Cell* **176**, 1432-1446 e1411 (2019). https://doi.org:10.1016/j.cell.2019.01.049

73 Robinson, A. D., Eich, M. L. & Varambally, S. Dysregulation of de novo nucleotide biosynthetic pathway enzymes in cancer and targeting opportunities. *Cancer letters* **470**, 134-140 (2020). https://doi.org:10.1016/j.canlet.2019.11.013

74 Chen, J. *et al.* De novo nucleotide biosynthetic pathway and cancer. *Genes Dis* **10**, 2331-2338 (2023). https://doi.org:10.1016/j.gendis.2022.04.018

75 Cerami, E. *et al.* The cBio cancer genomics portal: an open platform for exploring multidimensional cancer genomics data. *Cancer discovery* **2**, 401-404 (2012). https://doi.org:10.1158/2159-8290.CD-12-0095

76 Gao, J. *et al.* Integrative analysis of complex cancer genomics and clinical profiles using the cBioPortal. *Science signaling* **6**, pl1 (2013). https://doi.org:10.1126/scisignal.2004088

77 Kadariya, Y. *et al.* Mice heterozygous for germ-line mutations in methylthioadenosine phosphorylase (MTAP) die prematurely of T-cell lymphoma. *Cancer Res* **69**, 5961-5969 (2009). https://doi.org:10.1158/0008-5472.CAN-09-0145

78 Bertino, J. R., Waud, W. R., Parker, W. B. & Lubin, M. Targeting tumors that lack methylthioadenosine phosphorylase (MTAP) activity: current strategies. *Cancer biology & therapy* **11**, 627-632 (2011).

79 Alhalabi, O. *et al.* MTAP deficiency creates an exploitable target for antifolate therapy in 9p21-loss cancers. *Nature communications* **13**, 1797 (2022). https://doi.org:10.1038/s41467-022-29397-z

80 Chang, W. H. *et al.* MTAP deficiency contributes to immune landscape remodelling and tumour evasion. *Immunology* **168**, 331-345 (2023). https://doi.org:10.1111/imm.13587

Author Contributions

Conception and design: J. Yu, Y He, J Huang

Methodology development: J Yu, C Jin, C Pirozzi, X Gao, Y He

Data acquisition: J Yu, C Jin, C Su, D Moon, M Sun, X Jiang, N Tserentsoodol, C Pirozzi, X Gao, Y He

Data analysis and interpretation: J Yu, C Jin, C Su, D Moon, X Gao, Y He, J Huang

Writing, reviewing, and revision of the manuscript: J Yu, C Jin, C Su, D Moon, M Sun, H Zhang, X Jiang, N Tserentsoodol, M Bowie, C Pirozzi, DJ George, R Wild, X Gao, D Ashley, Y He, J Huang

Administrative, technical, or material support: J Yu, C Jin, C Su, D Moon, M Sun, H Zhang, X Jiang, F Zhang, N Tserentsoodol, M Bowie, C Pirozzi, DJ George, R Wild, X Gao, D Ashley, Y He, J Huang

Study supervision: Y. He, D Ashley, J Huang

Acknowledgements We thank Duke Cancer Center Isolation Facility for the support of experiments involving animal models. We thank Dr. Yasheng Gao and the Duke Light Microscopy Core Facility for assisting with imaging experiments, Drs. Darrell Bigner and Vidyalakshmi Chandramohan (Duke University) for sharing reagents, and Dr. Zhiguang Huang for his help with IHC assays. The work was supported by grants from the National Institutes of Health (5R01-CA260726) and the Prostate Cancer Foundation to J.H. We also acknowledge funding support from The Uncle Kory Foundation to Y.H. and NIH/NCI grant R00 CA237618, the USDA 3092-51000-064-05 and Cancer Prevention and Research Institute of Texas (PR210056, CPRIT) Scholar award in Cancer Prevention and Research to X.G.

Competing Interests J.H is a consultant for or owns shares in the following companies: Artera, Kingmed Diagnostics, MoreHealth, OptraScan, York Biotechnology, Chimigen Bio, Pfizer and Sisu Pharma.

Figure legends

Fig. 1. Prostate cancer cells stressed by purine shortage reprogram their purine biosynthesis machinery as an adaptive response. (A) PC3 cells were treated with DRP-104 and subjected to metabolic profiling. Analysis of the altered metabolites in DRP-104-treated cells vs. the control-treated cells showed that purines were among those that were most strongly affected. **(B)** Tumor cells were treated with indicated agents and the relative cell proliferation was monitored by IncuCyte. For DRP-104, 1 µM (for C4-2) or 2 µM (for PC3) were used. Exogenous purines used included adenosine plus guanosine (each at concentration ranging from 30-100 µM). Data are depicted as mean ± SD. **(C)** Treatment-naïve (parental) or DRP-104-adaptive C4-2 cells were treated with Enzalutamide (Enza) and cell proliferation was determined. Similar results were obtained in LNCaP cell lines treated with hormone depletion (by using charcoal-stripped FBS). Data are depicted as mean ± SEM. **(D)** Cells used in (C) were subjected to immunoblot assays. **(E)** Treatment-naïve or DRP-104-adaptive C4-2 cells were treated with vehicle or with low doses of Docetaxel (Dtxl) (e.g., 0.1 nM) and the relative cell proliferation was determined. $***p<0.001$. **(F)** Treatment-naïve or DRP-104-adaptive C4-2 cells were subjected to purinosome formation assays using FGAMS-EGFP as the biomarker. (**G**) DRP-104-adaptive C4-2 cells were treated with vehicle or with Docetaxel (Dtxl, 1 nM) transiently and the abundance of purinosomes was determined. Representative images and the quantification were shown. Similar results were obtained in PC3 cell lines. **(H)** DRP-104-adaptive C4-2 cells were treated with indicated agents and their relative growth was shown (day 4 data). $***p<0.001$.

Fig. 2. Cancer cells respond to DRP-104 treatment by promptly forming purinosomes. Cancer cell lines were transfected with exogenous FGAMS-EGFP expressing plasmid and subjected to DRP-104 treatment (day 0), and the presence of purinosomes (FGAMS-EGFP foci) were determined (day 2). Alternatively, tumor cells were treated with DRP-104 (day 0), and the presence of purinosomes was detected by anti-PAICS

immunofluorescent staining and confocal microscopy analysis (day 2). Representative images (**A, C**) and quantifications (**B, D**) were shown. ***p<0.001.

Fig. 3. MTAP-dependent Purine salvage is a critical source of purine supply in tumor cells. (A) Prostate cancer cells were treated with DRP-104 (4 µM, 2 days) and subjected to metabolic profiling to identify metabolites that were affected. Pathway topology analysis was performed to identify metabolism pathway that were significantly altered. **(B-C)** C4-2 cells expressing exogenous FGAMS-EGFP were subjected to MTDIA treatment (day 0), and the presence of purinosomes was detected (day 2). Alternatively, cells were treated with MTDIA (day 0), and the presence of purinosomes was detected by anti-PAICS immunofluorescent staining and confocal microscopy analysis (day 2). Representative images and quantifications were shown. **(D-E)** CT-2A cells transfected with exogenous FGAMS-EGFP expressing plasmid and subjected to MTDIA treatment (5 µM, day 0), and the presence of purinosomes was detected (day 2). Separately, *Mtap*-ko CT-2A cells were used for similar FGAMS-EGFP-based purinosome detection. Representative images (D) and quantifications (E) were shown. **(F-H)** Treatment-naïve (parental) and **(I-K)** DRP-104-adaptive C4-2 lines were treated with vehicle, MTDIA (3 µM), Docetaxel (0.1 nM) or MTDIA plus Docetaxel and cell growth was determined. Data are depicted as mean ± SEM. ***p<0.001.

Fig. 4. MTAP deficiency sensitizes tumor cells to DRP-104 treatments. (A-B) Tumor cells were treated with indicated agents and the relative cell proliferation was monitored by IncuCyte. 2 µM of DRP-104 was used for all cell lines; concentrations of 5’dAdo used varied from 10-60 µM, yielding consistent results; concentration of MTDIA used was 3 µM. Data are depicted as mean ± SD. **(C)** PC3 cells were treated with indicated agents and their growth was determined by IncuCyte (4, 30 and 3 µM was used for DON, 5’dAdo and MTDIA, respectively). Data are depicted as mean ± SD. **(D)** Immunoblots confirmed the knockout of *MTAP* in C4-2 cell line. **(E)** C4-2-derived CRISPR control (*MTAP*-intact) and *MTAP*-ko cell lines were treated with vehicle control or with DRP-104 or DON, and relative cell growth (compared to the vehicle control) on day 6 post treatment was shown. **(F)** *Mtap*-intact (parental) and *Mtap*-null CT-2A lines were treated with DRP-104 or DON and their growth was determined (relative cell growth on day 6 and day 5 were shown for DRP-105 and DON treatments, respectively; standard deviations were denoted). For the CT-2A cell lines, exogenous 5’dAdo (10 µM) was supplied in the media to ensure sufficient MTAP substrate was present. *p<0.05, **p<0.01, ***p<0.001.

Fig. 5. Combining DRP-104 with MTDIA yields superior therapeutic efficacy in an immunocompetent tumor model. (A-C) TrampC2-derived tumor-bearing wildtype C57BL/6 male mice were treated with indicated agents and tumor volumes were determined during the two weeks’ treatment period (n=6 mice per arm). Data are depicted as mean ± SEM in (A). Images and weights of tumors at Day 14 (after 6 treatments) were shown (B) and (C). **(D)** Representative images of tumors that were harvested after two weeks’ treatments. **(E)** IHC

staining for CD3, CD8α, PD-1 and PD-L1 in the harvested tumors. ns: no significant, *$p<0.05$, **$p<0.01$, ***$p<0.001$.

Fig. 6. DRP-104 treatments result in activated cGAS-STING pathway. (A) PC3-derived tumor bearing mice were treated with indicated agents and tumor volumes were monitored during the treatment period. Data are depicted as mean ± SEM. **(B-C)** PC3-derived xenografts treated with vehicle or with DRP-104 (with or without MTDIA) were used for anti-□H2AX and anti-p-IRF3 IHC and (B) representative images and (C) quantifications were shown. **(D)** ISRE reporter-tagged PC3 cells were treated with indicated agents and the reporter signal was monitored by IncuCyte (poly I:C, a known stimulator of the ISRE activity, was included as a positive control). Integrated fluorescent reporter signaling was normalized by cell confluences as determined by IncuCyte. **(E)** ISRE reporter-tagged C4-2 cells were treated with indicated agents and the reporter signal was determined. **(F-G)** ISRE reporter-tagged, *Mtap*-null derivative CT-2A cell line (F) and parental (*Mtap*-intact) CT-2A line (G) were treated with indicated agents and the reporter signal was monitored by IncuCyte (IFN□ was included as a positive control; day 4 data was shown in F). **(H)** C4-2 cells were treated with indicated agents and the expression of marker genes in the cGAS-STING pathway, *IFNB1* and *CCL5*, was determined. (I) *Mtap*-null CT-2A cells were treated with indicated agents and the expression of marker genes in the cGAS-STING pathway, *Ifnb1* and *Ccl5*, was determined. carbo.: carboplatin. n.s.: not significant, *$p<0.05$, **$p<0.01$, ****$p<0.0001$.

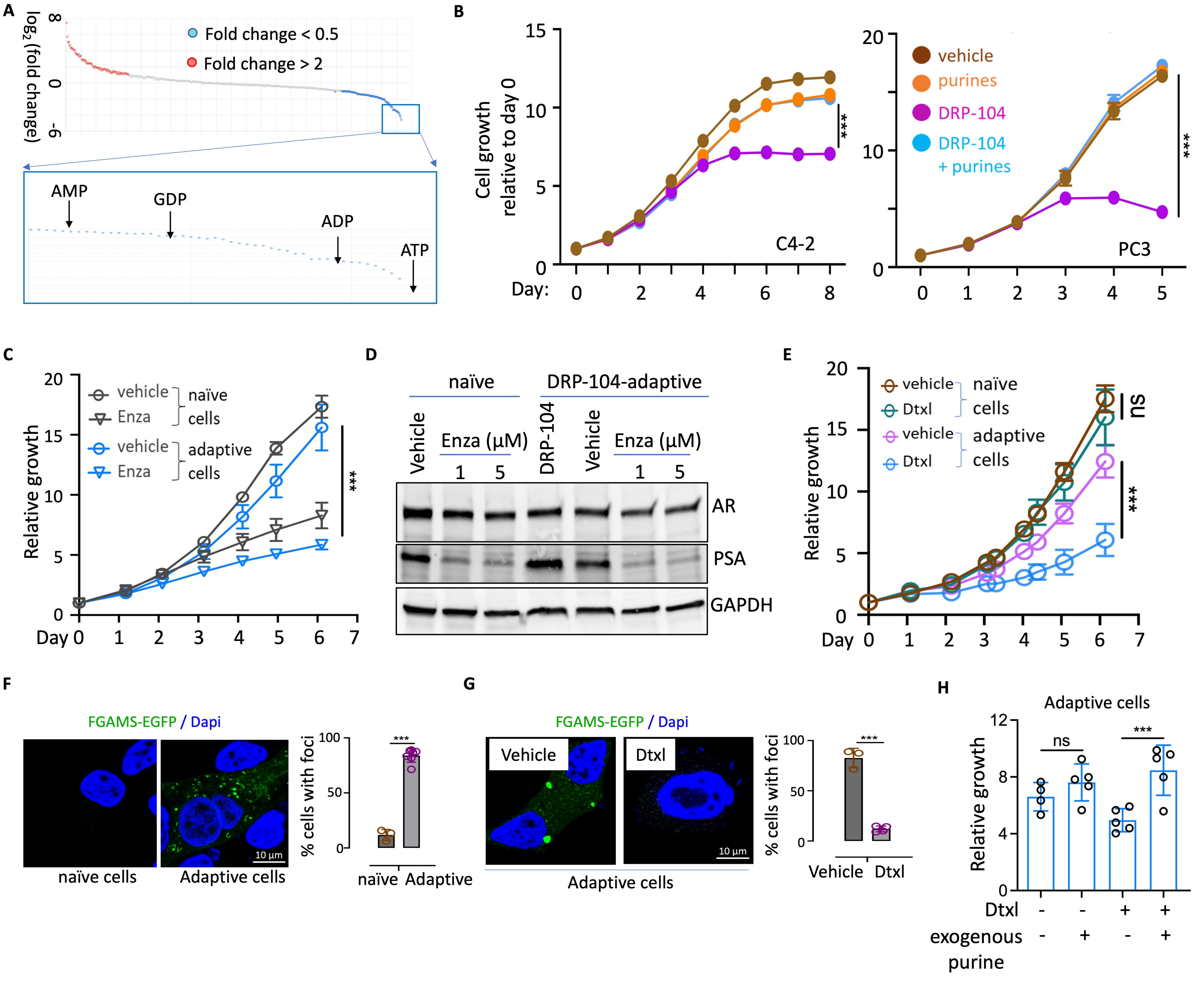
A
log2 (fold change)
8
0
-6
Fold change < 0.5
Fold change > 2
AMP
GDP
ADP
ATP
B
Cell growth relative to day 0
15
10
5
0
Day:
0
2
4
6
8
***
C4-2
20
10
0
0
1
2
3
4
5
vehicle
purines
DRP-104
DRP-104 + purines
***
PC3
C
Relative growth
20
15
10
5
0
Day 0
1
2
3
4
5
6
7
vehicle
Enza
naïve cells
vehicle
Enza
adaptive cells
***
D
naïve
DRP-104-adaptive
Vehicle
Enza (µM)
1
5
DRP-104
Vehicle
Enza (µM)
1
5
AR
PSA
GAPDH
E
Relative growth
20
15
10
5
0
Day 0
1
2
3
4
5
6
7
vehicle
Dtxl
naïve cells
vehicle
Dtxl
adaptive cells
ns
***
F
FGAMS-EGFP / Dapi
10 µm
naïve cells
Adaptive cells
% cells with foci
100
50
0
***
naïve
Adaptive
G
FGAMS-EGFP / Dapi
Vehicle
Dtxl
10 µm
Adaptive cells
% cells with foci
100
50
0
***
Vehicle
Dtxl
H
Adaptive cells
Relative growth
12
8
4
0
ns
***
Dtxl
-
-
+
+
exogenous purine
-
+
-
+

Fig. 1

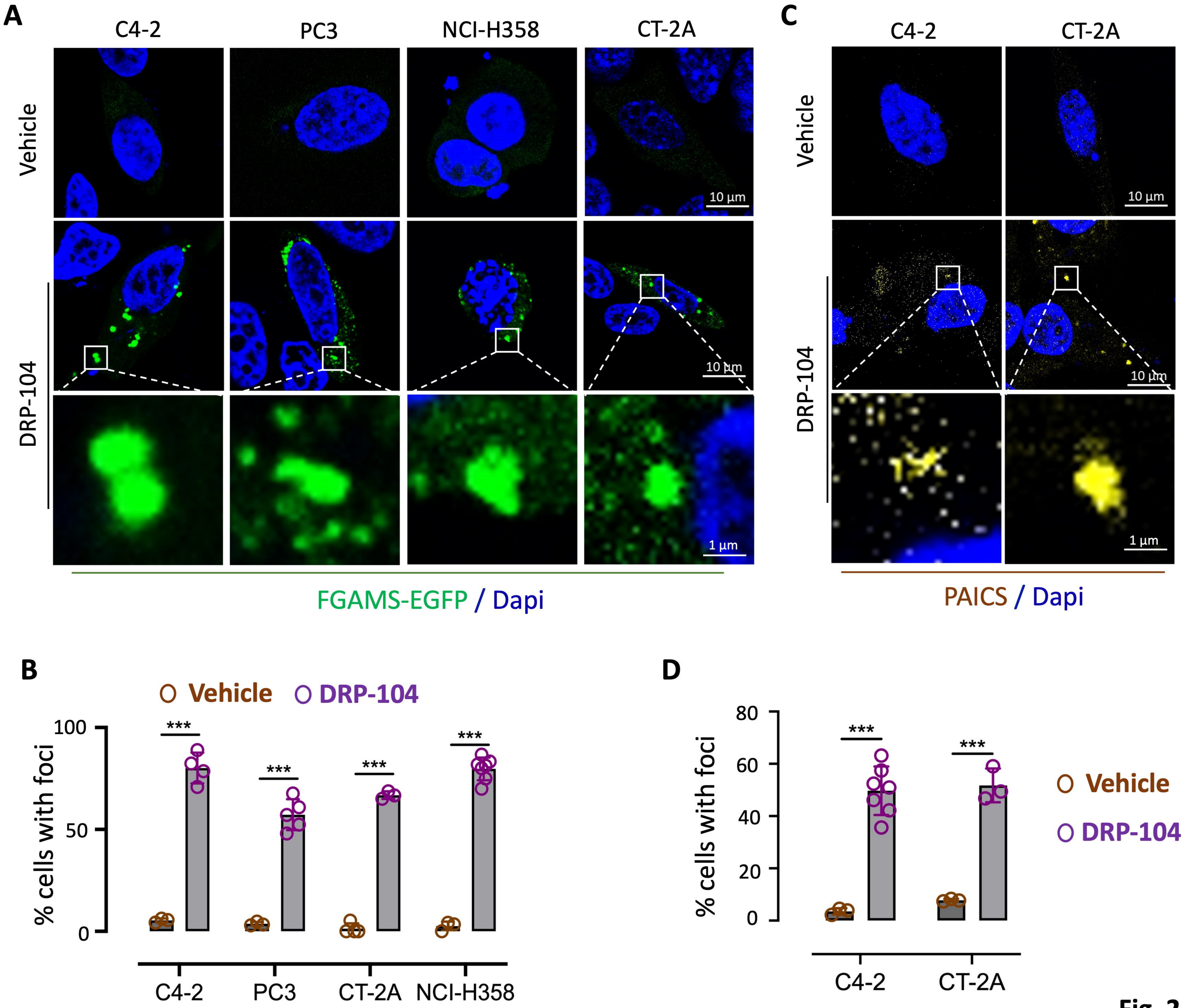
A
C4-2
PC3
NCI-H358
CT-2A
Vehicle
DRP-104
10 µm
10 µm
1 µm
FGAMS-EGFP / Dapi
C
C4-2
CT-2A
Vehicle
DRP-104
10 µm
10 µm
1 µm
PAICS / Dapi
B
Vehicle
DRP-104
% cells with foci
100
50
0
***
***
***
***
C4-2
PC3
CT-2A
NCI-H358
D
% cells with foci
80
60
40
20
0
***
***
Vehicle
DRP-104
C4-2
CT-2A

Fig. 2

A
Purine metabolism
-log10 (p-value)
p-value<0.05
Impact value
(C4-2: MTDIA vs Vehicle)
Purine metabolism
-log10 (p-value)
p-value<0.05
Impact value
(PC3: MTDIA vs Vehicle)
B
Vehicle
MTDIA
FGAMS-EGFP / Dapi
PAICS / Dapi
10 µm
1 µm
C
FGAMS-EGFP
PAICS (endogenous)
% cells with foci
***
***
Vehicle MTDIA
Vehicle MTDIA
D
Parental CT-2A (Mtap-intact)
Vehicle
MTDIA
Mtap-ko
10 µm
1 µm
FGAMS-EGFP / Dapi
E
CT-2A
% cells with foci
***
***
Vehicle MTDIA Mtap-ko
Mtap-intact
F
Vehicle
MTDIA
ns
Relative growth
Day
G
Vehicle
Docetaxel
ns
Relative growth
H
Vehicle
MTDIA+ Docetaxel
***
Relative growth
I
Vehicle
MTDIA
***
Relative growth
Day
J
Vehicle
Docetaxel
***
Relative growth
K
Vehicle
MTDIA+ Docetaxel
***
Relative growth

Fig. 3

A
C4-2
PC3
Relative growth
Day:
Vehicle
5’dAdo
DRP-104
DRP-104 + 5’dAdo
*
***
B
C4-2
PC3
Relative growth
Day:
Vehicle
MTDIA
DRP-104
DRP-104 + MTDIA
***
***
**
*
C
Vehicle
5’dAdo
DON
DON + 5’dAdo
Relative growth
Day:
***
Vehicle
MTDIA
DON
DON + MTDIA
***
**
D
MTAP-intact
MTAP -ko
MTAP
β-Actin
E
MTAP-intact
MTAP-Ko
Relative growth
ns
**
***
***
**
*
Vehicle
1
2
4
2
4
DRP-104 (μM)
DON (μM)
F
Normalized cell# relative to control
n.s.
*
*
***
***
***
DRP-104 (μM): 0 2 4 8 0 2 4 8
Mtap-intact
Mtap-null
Normalized cell# relative to control
n.s.
**
***
***
****
****
DON (μM): 0 2 4 8 0 2 4 8
Mtap-intact
Mtap-ko

Fig. 4

A
Vehicle
MTDIA
DRP-104
DRP-104
+ MTDIA
Tumor volume (mm^3)
500
400
300
200
100
0
0
2
5
7
9
12
14
Days post treatment
***
***
B
Vehicle
MTDIA
DRP-104
DRP-104
+MTDIA
C
Tumor weight (g)
0.4
0.3
0.2
0.1
0.0
NS
*
*
*
Vehicle
MTDIA
DRP-104
DRP-104
+MTDIA
D
Vehicle
MTDIA
DRP-104
DRP-104
+ MTDIA
H&E
E
Vehicle
MTDIA
DRP-104
DRP-104 + MTDIA
Percentage of positive cell
100
80
60
40
20
0
NS
***
***
NS
***
***
NS
***
p=0.09
NS
***
***
CD3
CD8α
PD-1
PD-L1

Fig. 5

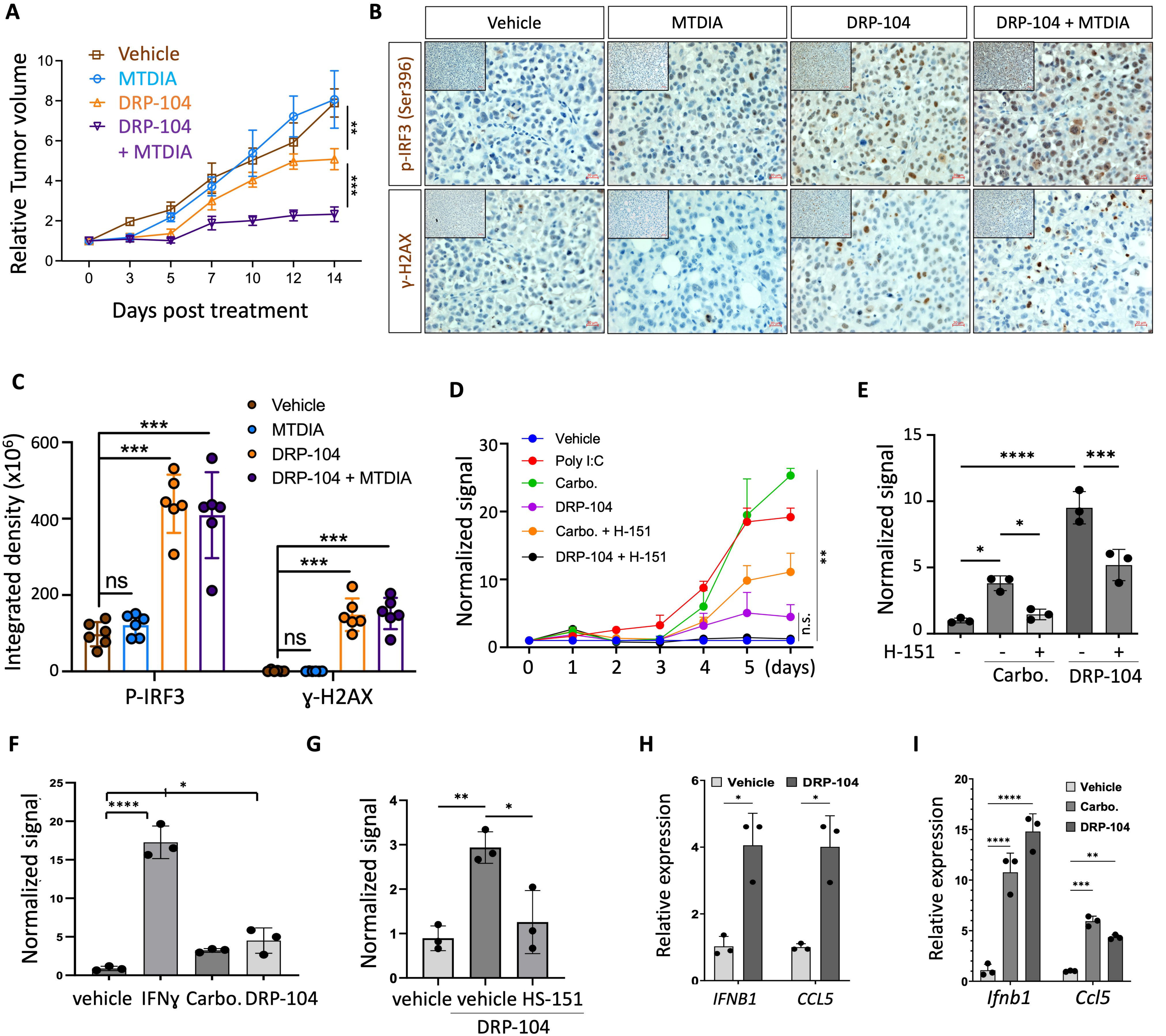
A
Relative Tumor volume
Days post treatment
0
3
5
7
10
12
14
10
8
6
4
2
0
Vehicle
MTDIA
DRP-104
DRP-104
+ MTDIA
**
***
B
Vehicle
MTDIA
DRP-104
DRP-104 + MTDIA
p-IRF3 (Ser396)
γ-H2AX
C
Integrated density (x10^6)
600
400
200
0
Vehicle
MTDIA
DRP-104
DRP-104 + MTDIA
***
***
ns
***
***
ns
P-IRF3
γ-H2AX
D
Normalized signal
30
20
10
0
0
1
2
3
4
5
(days)
Vehicle
Poly I:C
Carbo.
DRP-104
Carbo. + H-151
DRP-104 + H-151
**
n.s.
E
Normalized signal
15
10
5
0
****
***
*
*
H-151
-
-
+
-
+
Carbo.
DRP-104
F
Normalized signal
25
20
15
10
5
0
****
*
vehicle
IFNγ
Carbo.
DRP-104
G
Normalized signal
4
3
2
1
0
**
*
vehicle
vehicle
HS-151
DRP-104
H
Relative expression
6
4
2
0
Vehicle
DRP-104
*
*
IFNB1
CCL5
I
Relative expression
20
15
10
5
0
Vehicle
Carbo.
DRP-104
****
****
**
***
Ifnb1
Ccl5

Fig. 6